Yabu H, Shimomura M.	Preparation of self-organized mesoscale polymer patterns on solid substrate: continuous pattern formation from receding meniscus.	Adv Func Mater	15	575-581	2005
Yabu H, Shimomura M.	Simple fabrication of micro lens arrays.	Langmuir	21	1709-1711	2005
Yabu H, Shimomura M.	Single-step fabrication of transparent super hydrophobic porous polymer films.	Chem Mater	17	5231-5234	
Yabu H, Shimomura M.	Surface properties of self-organized honeycomb-patterned films.	Mol Cryst Liq Cryst (in press)			
Yabu H, Takebayashi M, Tanaka M, Shimomura M.	Super hydrophobic and lipophobic properties of self-organized honeycomb and pincushion structures.	Langmuir	21	3235-3237	2005

Yamamoto S, Tanaka M, Sunami H, Yamashita S, Morita Y, Shimomura M.	Relationship between adsorbed fibronectin and cell adhesion on a honeycomb-patterned film,	Surface Science. (in press)			
Yanagi T, Shimizu T, Abe R, Shimizu H.	Zinc dental fillings and palmoplantar pustulosis.	Lancet	366	1050	2005
Yanagi T, Shimizu T, Ujiie H, Tsuji-Abe Y, Abe R, Hige S, Shimizu H.	Improvement of mycosis fungoides during treatment of hepatitis C with peginterferon alfa-2b.	Arch Dermatol (in press)			
Young S, Wong M, Tabata Y, Mikos AG.	Gelatin as a delivery vehicle for the controlled release of bioactive molecules.	J Control Release (in press)			
Zhao Y, Shimizu T, Nishihira J, Koyama Y, Kushibiki T, Honda A, Watanabe H, Abe R, Tabata Y, Shimizu H.	Tissue regeneration using macrophage migration inhibitory factor-impregnated gelatin microbeads in cutaneous wounds.	Am J Pathol	167	1519-29	2005

IV. 研究成果の刊行物・別刷

Mutations in lipid transporter ABCA12 in harlequin ichthyosis and functional recovery by corrective gene transfer

Masashi Akiyama,[1] Yoriko Sugiyama-Nakagiri,[1] Kaori Sakai,[1] James R. McMillan,[2] Maki Goto,[1] Ken Arita,[1] Yukiko Tsuji-Abe,[1] Nobuko Tabata,[3] Kentaro Matsuoka,[4] Rikako Sasaki,[5] Daisuke Sawamura,[1] and Hiroshi Shimizu[1]

[1]Department of Dermatology, Hokkaido University Graduate School of Medicine, Sapporo, Japan. [2]Creative Research Initiative Sousei, Hokkaido University, Sapporo, Japan. [3]Division of Dermatology, Japanese Red Cross Sendai Hospital, Yagiyama, Tashiro, Sendai, Japan. [4]Division of Pathology and [5]Division of Dermatology, National Center for Child Health and Development, Okura, Setagaya, Tokyo, Japan.

Harlequin ichthyosis (HI) is a devastating skin disorder with an unknown underlying cause. Abnormal keratinocyte lamellar granules (LGs) are a hallmark of HI skin. ABCA12 is a member of the ATP-binding cassette transporter family, and members of the ABCA subfamily are known to have closely related functions as lipid transporters. ABCA3 is involved in lipid secretion via LGs from alveolar type II cells, and missense mutations in *ABCA12* have been reported to cause lamellar ichthyosis type 2, a milder form of ichthyosis. Therefore, we hypothesized that HI might be caused by mutations that lead to serious ABCA12 defects. We identify 5 distinct *ABCA12* mutations, either in a compound heterozygous or homozygous state, in patients from 4 HI families. All the mutations resulted in truncation or deletion of highly conserved regions of ABCA12. Immunoelectron microscopy revealed that ABCA12 localized to LGs in normal epidermal keratinocytes. We confirmed that ABCA12 defects cause congested lipid secretion in cultured HI keratinocytes and succeeded in obtaining the recovery of LG lipid secretion after corrective gene transfer of *ABCA12*. We concluded that ABCA12 works as an epidermal keratinocyte lipid transporter and that defective ABCA12 results in a loss of the skin lipid barrier, leading to HI. Our findings not only allow DNA-based early prenatal diagnosis but also suggest the possibility of gene therapy for HI.

Introduction

During the evolutionary process, when our ancestors left the safety of the aquatic environment, they developed a robust, protective mechanism or process in the skin that allowed adjustment to the new, dry environment; this is now known as keratinization. In humans, congenital defects involving skin keratinization cause a unique genodermatosis, ichthyosis (1, 2), which was named after the Greek word *ichthys*, meaning *fish*. Among the variety of types of ichthyosis, harlequin ichthyosis (HI) (Mendelian Inheritance of Man [MIM] 242500) is the most serious subtype (Figure 1); it is also the most severe congenital skin disorder of unknown etiology.

ABCA12 belongs to a large superfamily of ATP-binding cassette (ABC) transporters, which aid in the transport of various biomolecules across the cell membrane (3–5). The ABCA subfamily is thought to be important in lipid transport (6). ABCA12 is phylogenetically related to ABCA3, which is essential for alveolar surfactant lipid transport/secretion by lamellar granules (LGs) in type II alveolar lung cells. In skin, LGs are the most common secretory granules present in upper epidermal keratinocytes (7). Abnormal LGs are the most obvious characteristic findings in HI lesional epidermis. Furthermore, relatively minor missense mutations in *ABCA12* have been reported to underlie type 2 lamellar ichthyosis (MIM 601277), a milder form of ichthyosis (8). Thus, we hypothesized that *ABCA12* mutations leading to serious ABCA12 protein defects might underlie HI.

In the present study, we demonstrate that ABCA12 works as an epidermal keratinocyte lipid transporter and that defective ABCA12 results in a loss of the skin lipid barrier, leading to HI. We have found 5 distinct truncation, deletion, or splice-site mutations in 4 independent HI families. These mutations were present on both alleles of our HI patients, either in compound heterozygous or homozygous state. We demonstrate that *ABCA12* mRNA is expressed in normal human keratinocytes and that this expression is upregulated during keratinization. Our immunoelectron microscopic findings showed that ABCA12 protein localizes to LGs in the upper epidermal keratinocytes of human skin. Ultrastructural and immunofluorescent examination of human skin and cultured epidermal keratinocytes from HI patients who harbor *ABCA12* mutations revealed defective lipid secretion of LG lipid contents. In addition, using *ABCA12* corrective gene transfer in cultured HI keratinocytes, we have succeeded in restoring the normal ability of HI cells to secrete LG lipid.

Results

ABCA12 expression and localization in epidermal keratinocytes. To confirm the expression of *ABCA12* mRNA in human epidermal keratinocytes, we performed semiquantitative RT-PCR assays and demonstrated strong expression of *ABCA12* transcripts in cultured normal epidermal keratinocytes. To investigate the upregulation of *ABCA12* during keratinization under high-Ca^{2+} conditions, we evaluated the *ABCA12* transcript population against the GAPDH transcript using real-time RT-PCR. Calculation of the expres-

Nonstandard abbreviations used: ABC, ATP-binding cassette; CT, threshold cycle; HI, harlequin ichthyosis; LG, lamellar granule; MIM, Mendelian Inheritance of Man.

Conflict of interest: The authors have declared that no conflict of interest exists.

Citation for this article: *J. Clin. Invest.* **115**:1777–1784 (2005). doi:10.1172/JCI24834.

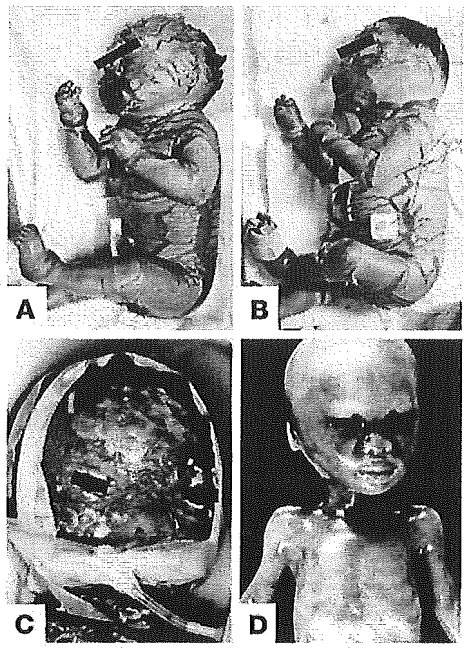

Figure 1
Clinical features of HI patients. (**A**) Patient 1 from family A harboring a homozygous mutation IVS23-2A→G in *ABCA12*. (**B**) Patient 2 from family B with compound heterozygous *ABCA12* mutations, IVS23-2A→G and 5848C→T (R1950X). (**C**) Patient 3 (family C) carrying compound heterozygous *ABCA12* mutations, 2021_2022del AA and 4158_4160delTAC (T1387del). (**D**) An affected fetus from family C aborted at 23 weeks' gestation showed no serious symptoms, although some abnormal keratinization was observed mainly on the cheeks and the perioral area.

sion ratios showed that *ABCA12* transcription was upregulated 4-fold after 1 week in high-Ca^{2+} culture. Furthermore, to confirm the expression of ABCA12 protein in the epidermis, we raised a polyclonal anti-ABCA12 antibody that recognizes an epitope near the C terminus of the ABCA12 polypeptide (residues 2567–2580) and performed immunostaining for ABCA12. ABCA12 was positive in the upper epidermal layers, mainly the granular layers, of normal human skin (Figure 2A); in contrast, there was an absence of immunolabeling in epidermal keratinocytes from HI patient 4 (Figure 2B), who harbors the homozygous truncation mutation R434X (see below). This mutation resulted in truncation of the protein, leading to loss of the epitope for the anti-ABCA12 antibody. These findings confirmed specificity of the anti-ABCA12 antibody. In the epidermis of patient 1, who harbors a homozygous splice acceptor site mutation IVS23-2A→G (see below), weak ABCA12 immunostaining was seen in the granular layer keratinocytes (Figure 2C). Immunoelectron microscopy revealed that ABCA12 protein was restricted to the LGs in the cytoplasm of epidermal keratinocytes (Figure 2, D and E). ABCA12-positive LGs were abundant close to the cell membrane and were observed fusing with the cell membrane to secrete their lipid content to the extracellular space of the stratum corneum (Figure 2F). These results indicate that ABCA12 is expressed in keratinocytes during keratinization and is likely to be involved in lipid transport into the extracellular space via LGs to form the stratum corneum lipid barrier (Figure 2G).

ABCA12 mutations in HI families. Full-length ABCA12 protein comprises 2595 amino acids and includes 2 ABCs containing 3 characteristic, highly conserved motifs (Walker A, Walker B, and active transport signature). In addition, there are 2 transmembrane domains, each consisting of 6 hydrophobic membrane-spanning helices. Mutational analysis of the 53 exons, including the exon-intron boundaries of the entire *ABCA12* gene, revealed 5 novel, distinct mutations in both alleles, either in compound heterozygous

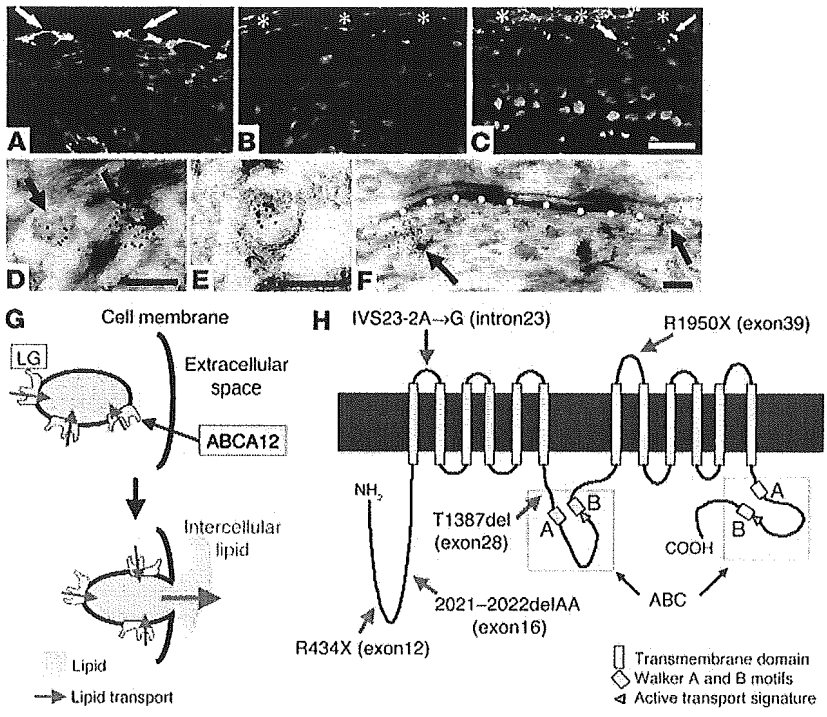

Figure 2
Localization and structure of ABCA12 protein and the sites of HI mutations. (**A**) ABCA12 protein (green) was localized in the cytoplasm of the upper epidermal keratinocytes (arrows) in healthy skin. (**B**) No ABCA12 immunolabeling was seen in the epidermis of patient 4. (**C**) Weak ABCA12 staining (arrows) was observed in the epidermis of patient 1. Asterisks indicate nonspecific staining in the stratum corneum. Red, nuclear counterstain. Scale bar: 10 μm. (**D–F**) By immunoelectron microscopy, ABCA12 protein (5 nm gold particles) was restricted to LGs (arrows) in the upper epidermal cell (**D**). Lamellar structures were apparent in some ABCA12-positive LGs (**E**). ABCA12-positive LGs (arrows) were observed close to the keratinocyte-cell membrane (white circles) and they fused with it to secrete their contents into the intercellular space (**F**). Scale bars: 0.2 μm. (**G**) Model of ABCA12 function in the skin. ABCA12 transports lipid into the LG, and ABCA12-positive LGs fuse with the cell membrane to secrete lipid into extracellular space to form the intercellular lipid layer. (**H**) Structure of ABCA12 protein and the 5 mutation sites (red arrows) in HI families. Dark-blue area, cell membrane; bottom of dark-blue area, cytoplasmic surface.

or homozygous state, in all patients from 4 HI families (Figure 2H). The mutations in patients were homozygous in the 2 consanguineous families and compound heterozygous in the 2 nonconsanguineous families (Figure 3). The mutations were verified in the heterozygous parents. Each of the three mutations, 1300C→T (R434X), 2021_2022delAA, and 5848C→T (R1950X), resulted in truncation of a highly conserved region of the ABCA12 protein. The deletion mutation 4158_4160delTAC led to an in-frame deletion of a highly conserved threonine residue at codon 1387 (T1387del) within the first ATP-binding domain of the ABCA12 protein (Figure 4D). A splice acceptor site mutation, IVS23-2A→G, was verified by RT-PCR in mRNA from the patient's cultured keratinocytes (Figure 4, A–C). RT-PCR products from the patient showed 2 splice pattern variants different from the normal splicing variant in which 1 mutant transcript loses a 9-bp sequence from exon 24, which results in a 3-amino acid deletion (Y1099_K1101del). These 3 amino acids are located between the transmembrane domains and are highly conserved (Figure 4D). The other mutant transcript lost a 170-bp sequence from exon 24, which led to a frameshift. All of these mutations are thought to seriously affect either the function or specific critical structures of the ABCA12 protein.

Disturbed lipid secretion in epidermis of HI patients. Morphological observations revealed extraordinarily thick stratum corneum (Figure 5A) and abnormal LG secretion in keratinocytes of the epidermis of HI patients (Figure 5, C and E). Ultrastructurally, the cytoplasm in the stratum corneum was congested with abnormal lipid-containing droplets and vacuoles that resembled immature LG-like vesicles. In the keratinocyte cytoplasm of the granular layer, no normal LGs were apparent.

Immunofluorescent staining showed that glucosylceramide, a major lipid component of LG (7, 9) and an essential component of the epidermal permeability barrier (10), was diffusely distributed throughout the epidermis of HI patients (Figure 5G); this contrasts with the restricted, intense distribution in the stratum corneum of healthy skin (Figure 5H).

Abnormal lipid secretion in keratinocytes of HI patients and recovery of ABCA12 function by corrective gene transfer. Keratinocytes from patient 1, cultured under high-Ca^{2+} conditions (2.0 mM), expressed only a small amount of mutated ABCA12 protein (Figure 6J). Culture of HI keratinocytes under high-Ca^{2+} conditions (2.0 mM) induced a large number of cells to exhibit intense glucosylceramide staining around the nuclei, and this glucosylceramide failed to localize to the periphery of the keratinocyte cytoplasm (congested pattern) (Figure 6, A and C). Conversely, culture of healthy keratinocytes in high-Ca^{2+} conditions resulted in a large proportion of cells with diffuse glucosylceramide staining throughout the cytoplasm (widely-distributed pattern) (Figure 6, B and D). This difference was most pronounced after 1 week in culture (Figure 6, C and D). Electron microscopic observation of HI keratinocytes cultured for 1 week in high-Ca^{2+} conditions revealed that LGs formed, although proper secretion of their contents was not observed (Figure 6E). This finding suggests defects in LG lipid transport. Double immunostaining for ABCA12 protein

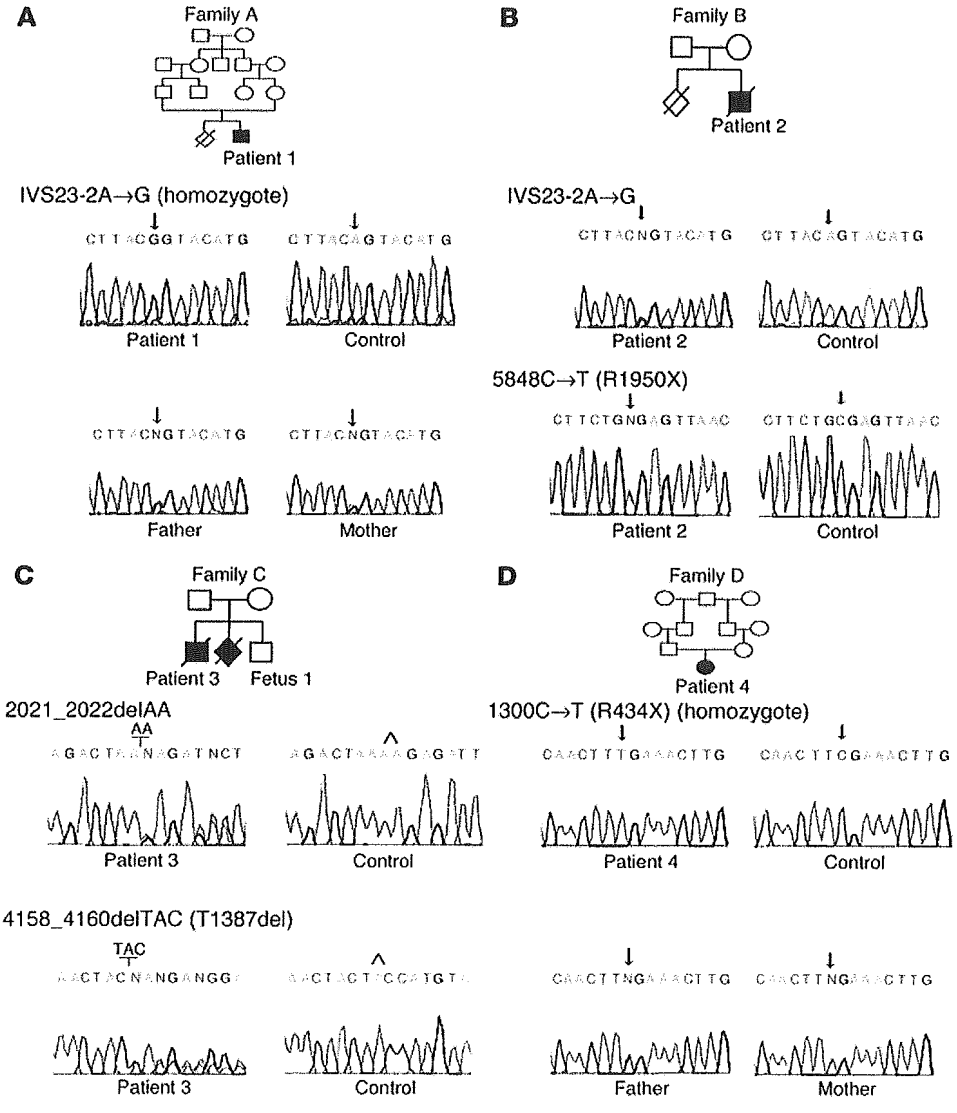

Figure 3
Families with HI and *ABCA12* mutations. (**A**) Patient 1 from family A was a homozygote for the mutation IVS23-2A→G, and both his parents were heterozygous carriers. (**B**) Patient 2 from family B was a compound heterozygote for the mutations IVS23-2A→G and 5848C→T (R1950X). (**C**) Patient 3 from family C was a compound heterozygote for the mutations 2021_2022delAA and 4158_4160delTAC (T1387del). (**D**) Patient 4 from family D was a homozygote for the mutation 1300C→T (R434X), and her 2 parents were heterozygous carriers.

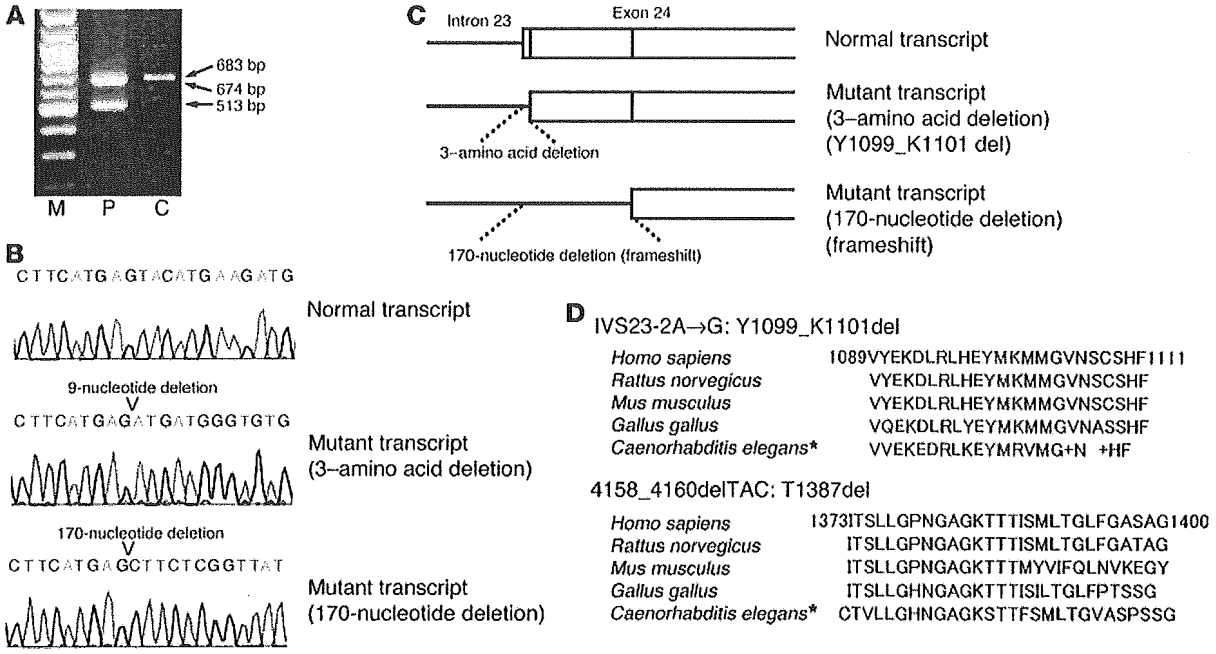

Figure 4

Verification of splice-site mutation IVS23-2A→G and conservation of residues deleted by mutations IVS23-2A→G and 4158_4160delTAC (T1387del). (**A**) RT-PCR analysis of mRNA fragments around the exon 23–24 boundary indicated that keratinocytes from patient 1 (lane P) showed 2 different mutant transcripts, 674 bp and 513 bp, which were shorter than the control transcript (683 bp) from healthy human keratinocytes (lane C). Lane M, markers. (**B**) Sequencing of the mutant transcripts and the control transcript revealed that 9 nucleotides and 170 nucleotides were deleted in mutant transcripts. (**C**) A 9-nucleotide deletion resulted in the loss of 3 amino acids from the N terminal sequence of exon 24 (Y1099_K1101del), and the 170-nucleotide deletion led to a frameshift. (**D**) ABCA12 amino acid sequence alignment shows the level of conservation in diverse species of the amino acids, Y1099_K1101 and T1387 (red characters), which were deleted by mutations in HI families. Asterisks indicate ABC (abt-4).

and glucosylceramide clearly demonstrated that, before genetic correction of ABCA12, keratinocytes from patient 1 with a low expression of mutated ABCA12 protein showed a congested glucosylceramide distribution pattern (Figure 6, J–L). After genetic correction, however, the HI patient's keratinocytes, now expressing normal ABCA12, showed a normal, widely-distributed pattern of glucosylceramide staining (Figure 6, M–O). Corrective ABCA12 gene transfer into cultured HI keratinocytes resulted in a significant increase in number of cells exhibiting the widely-distributed pattern of glucosylceramide staining from 6.98% ± 3.33% (control nontransfected patients' cells) to 16.70% ± 2.14 % (transfected patients' cells) (Student's t test, $P < 0.02$) (Figure 6P). These results clearly indicate that an ABCA12 deficiency leads to defective LG lipid transport into the intercellular space in HI patients, both in the epidermis and in cultured keratinocytes.

Discussion

An abnormal synthesis or metabolism of the LG lipid contents was previously suspected as being a possible pathogenetic mechanism underlying HI (11, 12). Here, we demonstrate that a severe ABCA12 deficiency causes defective lipid transport via LG in keratinizing epidermal cells, resulting in the HI phenotype.

The ABC transporter superfamily is one of the largest gene families, encoding a highly conserved group of proteins involved in energy-dependent active transport of a variety of substrates across membranes, including ions, amino acids, peptides, carbohydrates, and lipids (3–5, 13). ABC transporters have nucleotide-binding folds located in the cytoplasm and utilize energy from ATP to transport substrates across the cell membrane (3–5). ABC genes are widely dispersed throughout the eukaryotic genome and are highly conserved between species (6). The ABCA subfamily, of which the *ABCA12* gene is a member, comprises 12 full transporter proteins and 1 pseudogene (ABCA11). The ABCA subclass has received considerable attention (14) because mutations in these genes have been implicated in several human genetic diseases (15–19).

The ABCA1 protein is mutated in the following recessive disorders involving cholesterol and phospholipid transport: Tangier disease (MIM 205400), familial hypoalphalipoproteinemia (MIM 604091), and premature atherosclerosis, depending on the site of the mutations in the protein (17–19). The ABCA4 protein is mutated in Stargardt disease (MIM 248200) as well as in some forms of autosomal recessive retinitis pigmentosa (MIM 601718) and in the majority of cases of autosomal recessive cone-rod dystrophy (MIM 604116), depending on the mutation site or the combination of mutation types (15, 20). Heterozygous mutations in *ABCA4* have also been implicated in some cases of macular degeneration (MIM 153800) (16, 20). In a relatively mild type of congenital ichthyosis (lamellar ichthyosis type 2), 5 *ABCA12* mutations were reported in 9 families, and all 5 of these mutations were missense mutations that resulted in only 1 amino acid alteration (8). In the present series of HI patients, no *ABCA12* missense mutations were identified, and most of the defects led to severe truncation of the ABCA12 peptide, affecting important nucleotide-binding fold domains and/or transmembrane domains. The other, nontrun-

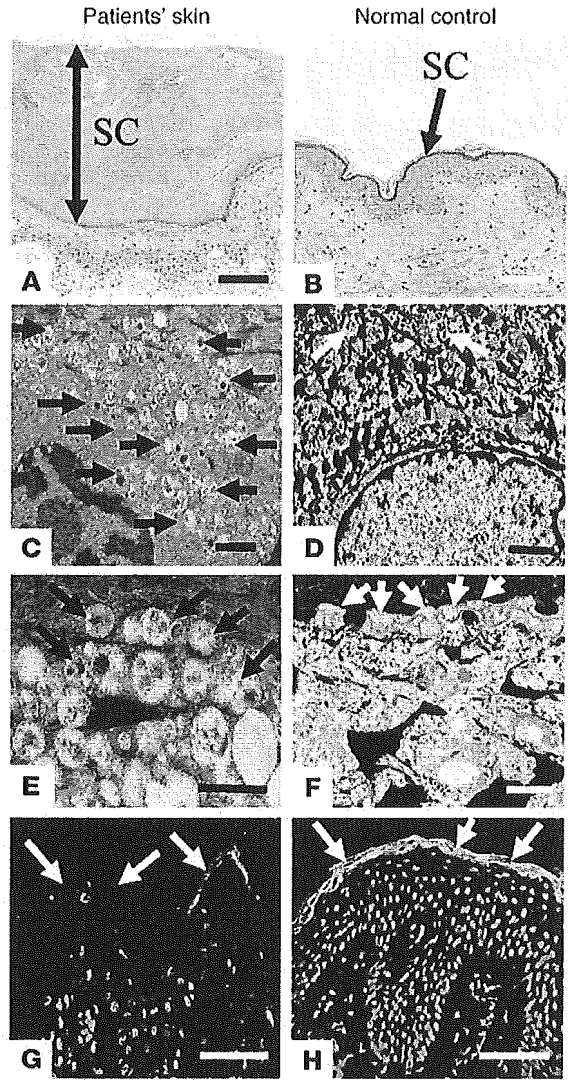

Figure 5
Extremely thick stratum corneum and severe disruption of the secretion of LGs in the ABCA12-deficient skin of the present series of HI patients. (**A**) Strikingly thick stratum corneum (SC; double arrow) in the patient's skin. (**B**) Control epidermis showing normal, stratum corneum (arrow). (**C**) By electron microscopy, LG secretion was disturbed, and many abnormal immature (lacking proper lamellar structures) LGs (arrows) were observed in the keratinocytes. (**D**) In control skin, LGs (arrows) were distributed in a gradually increasing pattern toward the plasma membrane. (**E**) Abnormal HI LGs (arrows) were localized close to the cell membrane, but not secreted. (**F**) LGs were secreted into the extracellular space (arrows). (**G**) Patient's epidermis including stratum corneum (arrows) showed diffuse staining for glucosylceramide (green), a lipid component of LGs. (**H**) Glucosylceramide staining (green) was restricted and intense in the stratum corneum (arrows) of normal skin. Red, nuclear stain. Scale bars: 50 μm (**A**, **B**, **G**, **H**); 1 μm (**C**, **D**); 0.5 μm (**E**, **F**).

cation mutations in HI were deletion mutations affecting highly conserved *ABCA12* sequences (Figure 4D). Thus, it is thought that only truncation or conserved region deletion mutations that seriously affect the function of the ABCA12 transporter protein lead to the HI phenotype. This is in contrast with diseases caused by mutations in other members of the ABCA family. Of *ABCA4* mutations causing Stargardt disease, 80% were missense, and many of these occurred in conserved domains of ABCA4 (21). Of *ABCA1* mutations resulting in Tangier disease, 60% were missense, located within the conserved domains of ABCA1 (22). In this context, *ABCA12* mutations underlying HI are unique in that these mutations are restricted to truncation or deletion mutations.

Patient 1 was homozygous for the splice acceptor site mutation IVS23-2A→G. This splice-site mutation was shown to lead to comparable amounts of 2 predicted transcripts, an inframe deletion of 3 amino acids, and a transcript with a 170-nucleotide deletion (frameshift) (Figure 4, A–C). Thus, it is still possible that patient 1 expresses some mutated ABCA12 protein. Indeed, expression of a small amount of ABCA12 protein, although mutated, was detected in the granular cells of the patient's epidermis and cultured keratinocytes by immunofluorescent staining (Figures 2C and 6J). This might have some relevance to the fact that patient 1 survived infancy and is still alive.

ABCA1 and ABCA4 are suspected transmembrane transporters for intracellular cholesterol/phospholipids (23–25) and protonated *N*-retinylidenephosphatidylethanolamines (26), respectively. *ABCA2*, *ABCA3*, and *ABCA7* mRNA levels have been reported to be upregulated by sustained cholesterol influx mediated by modified low-density lipoprotein (27, 28), suggesting that ABCA transporters are involved in transmembrane transport of endogenous lipids (23–26). Keratinocyte LGs are known lipid-transporting granules, and LG contents are secreted into the intercellular space, forming an intercellular lipid layer between the granular layer cells and keratinized cells in the stratum corneum, which is essential for the proper barrier function of human skin. Our results indicate that ABCA12 functions in the transport of endogenous lipid across the keratinocyte cell membrane into the stratum corneum intercellular space via LGs. Immunohistological and immunoelectron microscopic observations have indicated that ABCA3 is involved in lipid secretion of pulmonary surfactant in human lung alveolar type II cells (29). ABCA3 and ABCA12 are very closely related in the ABCA subfamily phylogenetic tree (30). It is interesting that the functions of both ABCA3 and ABCA12 are involved in alveolar surfactant and stratum corneum lipid secretion, respectively. This suggests that these 2 transporter systems are evolutionary adaptations to aid the respiratory system and the integument in a dry environment, developed as vertebrates left the aquatic environment and began terrestrial lives. HI skin that harbors serious defects in ABCA12 highlights the important role(s) of epidermal lipid transport in adapting human skin to a terrestrial, dry environment.

HI is one of the most severe of all genodermatoses and has a very poor prognosis. Thus, parents' request for prenatal diagnosis is to be taken seriously and with care. However, to our knowledge, the causative gene was not identified until now. For the last 20 years, prenatal diagnoses have only been performed by electron microscopic observation of fetal skin biopsy at a late stage of pregnancy (19–23 weeks estimated gestational age) (31–33). In this report, we have identified the causative gene in HI, which now makes possible DNA-based prenatal diagnosis using chorionic villus or amniotic fluid sampling at an earlier stage of pregnancy, with a lower procedural risk and a reduced burden on prospective mothers, similar to that of screening for other severe genetic disorders, including keratinization disorders (34). Furthermore, we have performed correc-

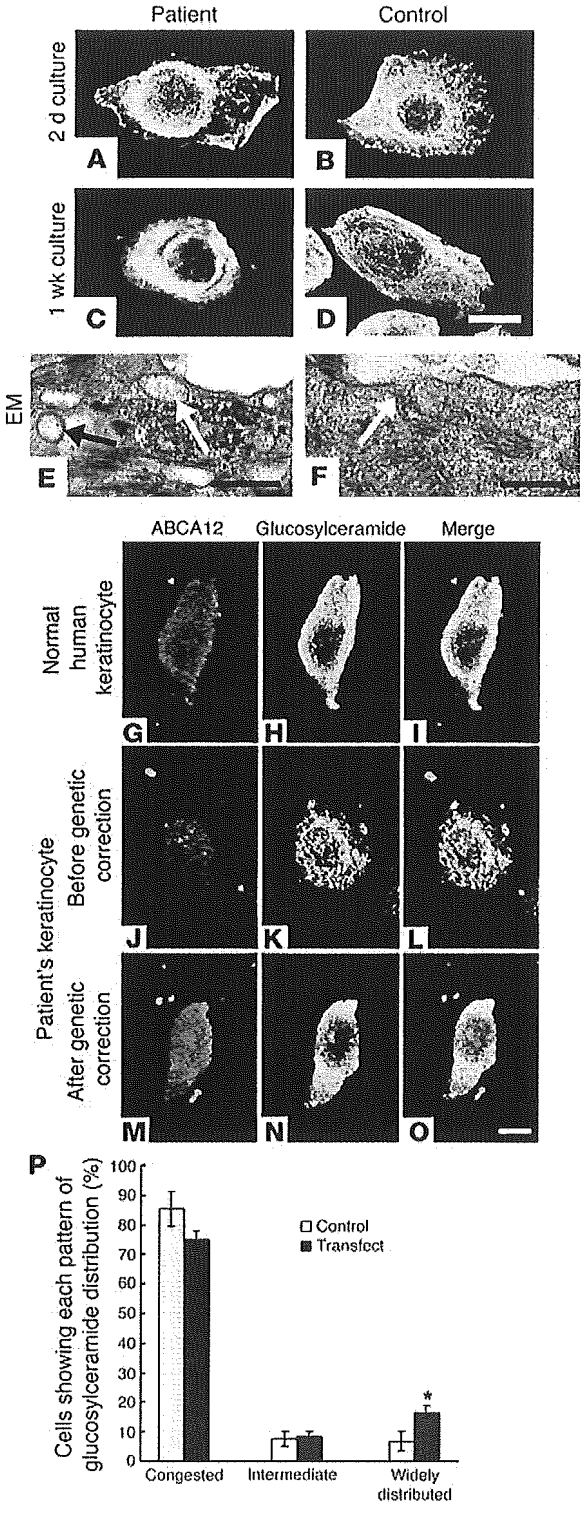

Figure 6

Cultured HI keratinocytes carrying *ABCA12* mutations showed abnormal congestion of lipid, and this phenotype was recovered by corrective *ABCA12* gene transfer. (**A–D**) HI keratinocytes cultured in high Ca^{2+} conditions showed that glucosylceramide, a major component of LG lipid, was distributed densely around the nuclei (in a congested pattern) (green, FITC). Control normal human keratinocytes showed a widely distributed, diffuse glucosylceramide staining pattern. (**E**) Electron microscopic (EM) observation revealed, in cultured HI keratinocytes, that apparently amorphous, electron lucent LG-like structures (arrows) formed, but were not secreted. (**F**) Normal secretion of LG contents (arrow) in a control keratinocyte. (**G–O**) Before genetic correction, an HI patient cell showed weak ABCA12 immunostaining (red, TRITC) and a congested pattern of glucosylceramide staining (green, FITC) (**J–L**). After genetic correction, an HI patient cell demonstrated stronger ABCA12 labeling (red) and a normal distribution pattern of glucosylceramide (green) (**M–O**), similar to those of a normal human keratinocyte (**G–I**). (**P**) Corrective gene transfer resulted in a statistically significant increase in the number of cells with completely normal, widely distributed glucosylceramide patterns. $^*P < 0.02$, Student's *t* test. Scale bars: 10 μm (**A–D**, **G–O**); 0.5 μm (**E**, **F**).

tive gene transfer in HI keratinocytes and succeeded in obtaining phenotypic rescue of a patient's cultured keratinocytes. These data provide significant clues that establish a strategic approach to HI gene therapy treatment. We believe that the genetic information presented in this study will be highly beneficial to our understanding of HI pathogenesis and in optimizing HI patient diagnosis, genetic counseling, care, and treatment.

Methods

Patients and families. Four HI patients, patients 1–4, and 1 affected fetus, fetus 1 (4 males, 1 female), from 4 independent families, families A–D, showed a serious collapse in the keratinized skin barrier (Figure 1). Family A and family D were consanguineous (marriage of first cousins). All the patients showed severe hyperkeratosis at birth and presented with generalized, thick scales over their entire body surface with the presence of marked fissuring. Severe ectropion, eclabium, and malformed pinnae were apparent in all cases. Patient 2 from family B died 3 days after birth. Patient 3 from family C died 15 days after birth, and an affected fetus from family C was terminated at the parents' request after a positive prenatal diagnostic skin test (33). After written, informed consent was obtained, blood samples were collected from each participating family member, and skin biopsy or autopsy specimens were obtained from the patients and the affected fetus. The study was given appropriate ethical approval by the Ethics Committee at Hokkaido University Graduate School of Medicine.

Mutation screening. Mutation analysis was performed in patients, an affected fetus, and other family members in the 4 families, as far as DNA samples would allow. Briefly, genomic DNA isolated from peripheral blood was subjected to PCR amplification, followed by direct automated sequencing using an ABI PRISM 3100 genetic analyzer (Applied Biosystems). Oligonucleotide primers and PCR conditions used for amplification of exons 1–53 of *ABCA12* were originally derived from the report by Lefèvre et al. (8) and were partially modified for the present study. The entire coding region, including the exon/intron boundaries for both forward and reverse strands from all patients, family members, and controls, were sequenced. No mutations were found in 100 control alleles from the Japanese population.

Verification of the splice acceptor site mutation. In order to verify the splice acceptor site mutation IVS23-2A→G, RT-PCR amplification of mRNA spanning the exon 23–24 boundary was performed using mRNA samples from cultured HI keratinocytes (see below). After RT-PCR amplification, direct sequencing of the products was performed.

Establishment of HI keratinocyte cell culture. A skin sample from patient 1 was processed for primary keratinocyte culture, and cells were grown according to standard procedures in defined keratinocyte serum-free medium (Invitrogen Corp.). Cultures were grown for several passages in low-Ca^{2+} (0.09 mM) conditions and then switched to high-Ca^{2+} (2.0 mM) conditions.

RT-PCR of ABCA12 mRNA. RT-PCR of ABCA12 mRNA was performed with Superscript 2 (Invitrogen Corp.) following the manufacturer's

instructions. Specific primers for PCR amplification were as follows: forward 5′-GAATTGCAAACTGGAAGGAACTCCC-3′ and reverse 5′-GAGTCAGCTAGGATTAGACAGC-3′. These primers were used for amplification of a 683-bp fragment around exon 23–24 boundary of normal cDNA.

Real time-PCR. For quantitative analysis of *ABCA12* expression levels, total RNA extracted was subjected to real-time RT-PCR using the ABI PRISM 7000 sequence detection system (Applied Biosystems). Specific primers/probes for human *ABCA12*, TaqMan Gene Expression Assay (HS00292421; Applied Biosystems) were used. Differences between the mean *CT* values of *ABCA12* and those of *GAPDH* were calculated as $\Delta CT_{sample} = CT_{ABCA12} - CT_{GAPDH}$ and those of the ΔCT for the cultured keratinocytes in the low Ca^{2+} condition as ($\Delta CT_{calibrator} = CT_{ABCA12} - CT_{GAPDH}$). Final results, the sample-calibrator ratio, expressed as *n*-fold differences in *ABCA12* expression were determined by $2^{-(\Delta CTsample - \Delta CTcalibrator)}$.

Cloning of ABCA12 and corrective gene transfer of HI keratinocytes. Using human keratinocyte cDNA as a template, overlapping clones of human *ABCA12* cDNA were amplified by PCR. A composite full-length cDNA was constructed, subjected to nucleotide sequencing, and subcloned into a pCMV-tag4B vector (Stratagene). The expression plasmid pCMV-tag4B-ABCA12 was transfected into HI keratinocytes using Lipofectamine reagent (Invitrogen Corp.) according to the manufacturer's recommendation. As a control, pCMV-tag4B was transfected into the cells. The transfected cells and control cells from patient 1 were stained with anti-glucosylceramide antibody, and the number of keratinocytes showing the 3 distinct types of glucosylceramide distribution patterns — congested, intermediate, and widely distributed — were assessed and calculated by 1 observer after viewing under a confocal laser scanning microscope, the Olympus Fluoview, FV300 confocal microscope (Olympus).

Morphological observation. Skin biopsy samples or cultured keratinocytes were fixed in 2% glutaraldehyde solution, postfixed in 1% OsO4, dehydrated, and processed for conventional electron microscopic observation.

Antibodies. Polyclonal anti-ABCA12 antibody was raised in rabbits using a 14-amino acid sequence synthetic peptide (residues 2567-2580) derived from the ABCA12 sequence (NM 173076) as the immunogen. The other primary antibody was mouse monoclonal anti-ceramide antibody (Alexis Biochemicals).

Immunofluorescent labeling. Immunofluorescent labeling was performed on frozen tissue sections and keratinocyte cultures as previously described (35). Fluorescent labeling was performed with FITC-conjugated secondary antibodies, followed by 10 μg/ml propidium iodide (Sigma-Aldrich) to counterstain nuclei. For double labeling, fluorescent labeling was performed with a TRITC-conjugated secondary antibody for the anti-ABCA12 antibody. The stained samples were observed under a confocal laser scanning microscope.

Postembedding immunogold electron microscopy. Normal human skin samples were obtained from skin surgical operations under fully informed consent and were processed for postembedding immunoelectron microscopy as previously described (36). Cyrofixed, cryosubstituted samples were embedded in Lowicryl K11M resin (Electron Microscopy Sciences). Ultrathin sections were cut and incubated with anti-ABCA12 antibody, a secondary linker antibody, and a 5-nm gold-conjugated antibody for immunogold labeling.

Acknowledgments

We thank members of the patients' families for their cooperation; Peter M. Elias for helpful discussion; Sadae Egawa, Haruhiko Sago, Judith Allanson, and Linlea Armstrong for their help; and Akari Nagasaki and Megumi Sato for their technical assistance. This work was supported in part by a Grant-in-Aid from the Ministry of Education, Science, Sports, and Culture of Japan (Kiban B 16390312; to M. Akiyama).

Received for publication February 23, 2005, and accepted in revised form April 12, 2005.

Address correspondence to: Masashi Akiyama, Department of Dermatology, Hokkaido University Graduate School of Medicine, N15 W 7, Sapporo 060-8638, Japan. Phone: 81-11-716-1161; Fax: 81-11-706-7820; E-mail: akiyama@med.hokudai.ac.jp.

1. Williams, M.L., and Elias, P.M. 1987.Genetically transmitted, generalized disorders of cornification; the ichthyoses. *Dermatol. Clin.* **5**:155–178.
2. Judge, M.R., McLean, W.H.I., and Munro, C.S. 2004. Disorders of keratinization. In *Rook's textbook of dermatology.* 7th edition. T. Burns, S. Breathnach, N. Cox, and C. Griffiths, editors. Blackwell Publishers. Oxford, United Kingdom. 34.1–34.111.
3. Allikmets, R., Gerrard, B., Hutchinson, A., and Dean, M. 1996. Characterization of the human ABC superfamily: isolation and mapping of 21 new genes using the expressed sequence tags database. *Hum. Mol. Genet.* **5**:1649–1655.
4. Dean, M., Rzhetsky, A., and Allikmets, R. 2001. The human ATP-binding cassette (ABC) transporter superfamily. *Genome Res.* **11**:1156–1166.
5. Borst, P., and Elferink, R.O. 2002. Mammalian ABC transporters in health and disease. *Annu. Rev. Biochem.* **71**:537–592.
6. Peelman, F., et al. 2003. Characterization of the ABCA transporter subfamily: identification of prokaryotic and eukaryotic members, phylogeny and topology. *J. Mol. Biol.* **325**:259–274.
7. Ishida-Yamamoto, A., et al. 2004. Epidermal lamellar granules transport different cargoes as distinct aggregates. *J. Invest. Dermatol.* **122**:1137–1144.
8. Lefèvre, C., et al. 2003. Mutations in the transporter ABCA12 are associated with lamellar ichthyosis type 2. *Hum. Mol. Genet.* **12**:2369–2378.
9. Vielhaber, G., et al. 2001. Localization of ceramide and glucosylceramide in human epidermis by immunogold electron microscopy. *J. Invest. Dermatol.* **117**:1126–1136.
10. Holleran, W.M., et al. 1993. Processing of epidermal glucosylceramides is required for optimal mammalian cutaneous permeability barrier function. *J. Clin. Invest.* **91**:1656–1664.
11. Dale, B.A., et al. 1990. Heterogeneity in harlequin ichthyosis, an inborn error of epidermal keratinization: variable morphology and structural protein expression and a defect in lamellar granules. *J. Invest. Dermatol.* **94**:6–18.
12. Milner, M.E., O'Guin, W.M., Holbrook, K.A., and Dale, B.A. 1992. Abnormal lamellar granules in harlequin ichthyosis. *J. Invest. Dermatol.* **99**:824–829.
13. Higgins, C.F. 1992. ABC transporters: from microorganisms to man. *Annu. Rev. Cell Biol.* **8**:67–113.
14. Klein, I., Sarkadi, B., and Varadi, A. 1999. An inventory of the human ABC proteins. *Biochim. Biophys. Acta.* **1461**:237–262.
15. Allikmets, R., et al. 1997. A photoreceptor cell-specific ATP-binding transporter gene (ABCR) is mutated in recessive Stargardt macular dystrophy. *Nat. Genet.* **15**:236–246.
16. Allikmets, R., et al. 1997. Mutation of the Stargardt disease gene (ABCR) in age-related macular degeneration. *Science.* **277**:1805–1807.
17. Brooks-Wilson, A., et al. 1999. Mutations in ABC1 in Tangier disease and familial high-density lipoprotein deficiency. *Nat. Genet.* **22**:336–345.
18. Rust, S., et al. 1999. Tangier disease is caused by mutations in the gene encoding ATP-binding cassette transporter 1. *Nat. Genet.* **22**:352–355.
19. Oram, J.F. 2002. Molecular basis of cholesterol homeostasis: lessons from Tangier disease and ABCA1. *Trends Mol. Med.* **8**:168–173.
20. Allikmets, R. 2000. Simple and complex ABCR: genetic predisposition to retinal disease. *Am. J. Hum. Genet.* **67**:793–799.
21. Lewis, R.A., et al. 1999. Genotype-phenotype analysis of a photoreceptor-specific ATP-binding cassette transporter gene, ABCR, in Stargardt disease. *Am. J. Hum. Genet.* **64**:422–434.
22. Huang, W., et al. 2001. Novel mutations in ABCA1 gene in Japanese patients with Tangier disease and familial high density lipoprotein deficiency with coronary heart disease. *Biochim. Biophys. Acta* **1537**:71–78.
23. Hayden, M.R., et al. 2000. Cholesterol efflux regulatory protein, Tangier disease and familial high-density lipoprotein deficiency. *Curr. Opin. Lipidol.* **11**:117–122.
24. Orso, E., et al. 2000. Transport of lipids from Golgi to plasma membrane is defective in Tangier disease patients and Abc1-deficient mice. *Nat. Genet.* **24**:192–196.
25. Schmitz, G., and Langmann, T. 2001. Structure, function and regulation of the ABC1 gene product. *Curr. Opin. Lipidol.* **12**:129–140.
26. Weng, J., et al. 1999. Insights into the function of Rim protein in photoreceptors and etiology of Stargardt's disease from the phenotype in abcr knockout mice. *Cell.* **98**:13–23.
27. Klucken, J., et al. 2000. ABCG1 (ABC8), the human homolog of the Drosophila white gene, is a regulator of macrophage cholesterol and phospholipid transport. *Proc. Natl. Acad. Sci. U. S. A.* **97**:817–822.
28. Kaminski, W.E., et al. 2001. Complete coding sequence, promoter region, and genomic structure

of the human ABCA2 gene and evidence for sterol-dependent regulation in macrophages. *Biochem. Biophys. Res. Commun.* **281**:249–258.
29. Yamano, G., et al. 2001. ABCA3 is a lamellar body membrane protein in human lung alveolar type II cells. *FEBS Lett.* **508**:221–225.
30. Annilo, T., et al. 2002. Identification and characterization of a novel ABCA subfamily member, ABCA12, located in the lamellar ichthyosis region on 2q34. *Cytogenet. Genome Res.* **98**:169–176.
31. Blanchet-Bardon, C., et al. 1983. Prenatal diagnosis of harlequin fetus [letter]. *Lancet.* 1:132.
32. Akiyama, M., Kim, D.-K., Main, D.M., Otto, C.E., and Holbrook, K.A. 1994. Characteristic morphologic abnormality of harlequin ichthyosis detected in amniotic fluid cells. *J. Invest. Dermatol.* **102**:210–213.
33. Akiyama, M., Suzumori, K., and Shimizu, H. 1999. Prenatal diagnosis of harlequin ichthyosis by the examinations of keratinized hair canals and amniotic fluid cells at 19 weeks' estimated gestational age. *Prenat. Diagn.* **19**:167–171.
34. Tsuji-Abe, Y., et al. 2004. DNA-based prenatal exclusion of bullous congenital ichthyosiform erythroderma at the early stage, 10-11 weeks' of pregnancy in two consequent siblings. *J. Am. Acad. Dermatol.* **51**:1008–1011.
35. Akiyama, M., et al. 1999. Periderm cells form cornified cell envelope in their regression process during human epidermal development. *J. Invest. Dermatol.* **112**:903–909.
36. Shimizu, H., McDonald, J.N., Kennedy, A.R., and Eady, R.A.J. 1989. Demonstration of intra- and extra-cellular localization of bullous pemphigoid antigen using cryofixation and freeze substitution for postembedding immuno-electron microscopy. *Arch. Dermatol. Res.* **281**:443–448.

Available online at www.sciencedirect.com
SCIENCE DIRECT®
ELSEVIER
Biomaterials 27 (2006) 1797–1802
Biomaterials
www.elsevier.com/locate/biomaterials

Biodegradable honeycomb-patterned film composed of poly(lactic acid) and dioleoylphosphatidylethanolamine

Yukako Fukuhira[a,*], Eiichi Kitazono[a], Takami Hayashi[a], Hiroaki Kaneko[a], Masaru Tanaka[b], Masatsugu Shimomura[c], Yoshihiko Sumi[a]

[a]*Department of Tissue Engineering Development, Innovation Research Institute, Teijin Ltd., 4-3-2, Asahigaoka, Hino, Tokyo 191-8512, Japan*
[b]*Creative Research Initiative Sousei, Hokkaido University, N21W10, Sapporo 001-0021, Japan*
[c]*Nanotechnology Research Center, Research Institute for Electronic Science, Hokkaido University, N21W10, Sapporo, 001-0021, Japan*

Received 9 May 2005; accepted 31 October 2005
Available online 15 November 2005

Abstract

Honeycomb-patterned films have been reported to be useful for scaffolds of cell culture in tissue engineering. In the present study, we investigated a new compound, dioleoylphosphatidylethanolamine (DOPE), a naturally derived phospholipid having unsaturated fatty acid moieties, as a surfactant for fabricating honeycomb-patterned poly(D,L-lactide) (PLA) film. Only DOPE among commercially available phospholipids was useful as a surfactant, and it showed good solubility in PLA/chloroform solution and an excellent property for fabricating honeycomb-patterned film (the concentration of DOPE was from 0.2% to 20% by weight based on the weight of PLA). The pore size of the honeycomb was uniform, and all pores were interconnected with each other. The contact angle of water on the honeycomb-patterned film was affected by the amount of DOPE. Time-of-flight secondary ion mass spectrometer (TOF-SIMS) data suggested that DOPE was concentrated on the surface of the honeycomb-patterned film. To investigate cell proliferation and adhesion on the honeycomb-patterned film, NIH3T3 fibroblast cells were cultured on the film. The NIH3T3 cells adhered well on the honeycomb-patterned PLA film with DOPE (PLA–DOPE) and showed good cell proliferation compared to that on honeycomb-patterned PLA film fabricated with a copolymer (CAP) of dodecylacrylamide and ω-carboxyhexylacrylamide (PLA–CAP).

These results suggest that the honeycomb-patterned PLA–DOPE can be applicable as a scaffold for cells with better profiles in comparison with PLA–CAP.

Keywords: Phospholipid; Honeycomb-patterned film; Polylactic acid; Cell adhesion; Surface modification; Tissue engineering

1. Introduction

In recent years, the micro-size structure has been widely applied to electronic materials [1], catalysts [2], the separator for blood cells [3,4], and cell culture substrates [5–7], etc. These are known to be prepared by lithography [8], soft lithography [9], phase separation of block copolymers [10], and so on. In regard to the application of the micro-size structure to the separator for blood cells or cell culture substrates, it is recognized that the surface structures of materials have considerable influence on the adhesion, migration and proliferation of cells. Since the micro-size structure on the material surface is important to control cell behavior, much attention has been directed toward technology for fabricating the material surface.

Some authors have reported that the honeycomb-patterned micro-size structure on a polymer surface can control cell activity arbitrarily. This honeycomb pattern was prepared by a simple casting method [11–13]. More particularly, the polymer solution was cast on a petri dish, water droplets self-assembled on the polymer solution by adding humid air, and the honeycomb pattern was observed on polymer film after drying. Cell proliferation and adhesion on the honeycomb pattern were influenced by the pore size of the honeycomb structure.

It is possible to produce a honeycomb structure on biodegradable polyester films made from poly(lactic acid)

*Corresponding author. Tel.: +81 42 586 8327; fax: +81 42 587 5511.
E-mail address: y.fukuhira@teijin.co.jp (Y. Fukuhira).

0142-9612/$ - see front matter © 2005 Elsevier Ltd. All rights reserved.
doi:10.1016/j.biomaterials.2005.10.019

or poly(ε-caprolactone) [3]. A honeycomb-patterned film on biodegradable polyester is useful as a cell culture substrate. The complex of cultured cells and honeycomb-patterned biodegradable polymer film is expected to be useful for tissue engineering. To form the honeycomb pattern on polymer film, a surfactant is essential to stabilize the water droplets and acts as a template of the honeycomb pattern on the surface of the polymer solution. The surfactant must have amphiphilicity, because it contributes to the stability of the water droplet at the polymer solution–water interface by forming a micelle-like structure.

Polymers having this property, such as the amphiphilic polymers and polyion complexes, can form the honeycomb structure by themselves [5–7,11]. Nevertheless, an amphiphilic poly (acrylamide) copolymer, CAP, which is derived from dodecylacrylamide and ω-carboxyhexylacrylamide, has been reported as the only surfactant useful for fabricating the honeycomb pattern on biodegradable polyester so far [3]. It is a synthetic polymer, and the metabolic pathway in the body has not been made clear. If a honeycomb-patterned film composed of biodegradable polyesters can be fabricated using a naturally derived or biodegradable surfactant, it can be used preferably as a scaffold for tissue engineering or prosthesis in the human body. However, that kind of surfactant for fabricating a honeycomb pattern on biodegradable polyesters has not been reported at all.

The purpose of this study was to investigate an optimal biodegradable surfactant for fabricating the honeycomb pattern on biodegradable polyester, Poly(D,L-lactic acid) (PLA) film. In this study, we focused on naturally derived phospholipids such as phosphatidylcholines (PC) and phosphatidylethanolamines (PE), and examined them as surfactants to fabricate the honeycomb structure on PLA film. The cell proliferation and adhesion on the PLA film was observed by using NIH3T3 cells.

2. Materials and methods

2.1. Fabrication of the honeycomb-patterned film

PLA (Mw = 200,000 [14], Lacty #9031, Shimadzu, Kyoto, Japan) was dissolved in chloroform (Wako Pure Chemical Industries Ltd., Osaka, Japan) at a concentration of 5 mg/mL at room temperature. Dioleoylphosphatidylethanolamine (DOPE) (COATSOME ME-8181, NOF Co., Tokyo, Japan) was added in various concentrations from 0.1% to 100% by weight based on the weight of PLA. Similarly, other phospholipids (DLPC, DMPC, DPPC, DSPC, DOPC, DMPE, DPPE, and DSPE) shown in Table 1, were added to the polymer solution by wt% concentration (5, 10 and 20 wt%). The honeycomb-patterned films were fabricated by casting the polymer solution under blowing with air (about 80% humidity, 1–8/min.) at room temperature in air of 30% humidity. The casting volume of the polymer solution was 5 mL/petri dish (10 cm in diameter). The honeycomb-patterned films for the cell culture were prepared on cover glasses (ϕ: 15 mm, Matsunami Glass Industrial Ltd., Tokyo, Japan), which were placed in the petri dishes, and produced the same pore size (3 μm). The pore size of the honeycomb-patterned film can be controlled by the temperature, humidity, gas flow rate, casting volume, and casting concentration [15]. The honeycomb-pattern was observed by an optical microscope (BX51, Olympus Co., Tokyo, Japan) and FE-SEM (S-5200, Hitachi High Technologies, Tokyo, Japan). The contact angles of the honeycomb-patterned films were measured (CA-S, Kyowa Interface Science, Saitama, Japan). The residual DOPE in the honeycomb-patterned film after ethanol washing was measured by ^{1}H-NMR (A-600, JEOL, Tokyo, Japan). The surface chemical composition of the honeycomb-patterned film was observed by Time-of-flight secondary ion mass spectrometer (TOF-SIMS IV, ION-TOF GmbH, Germany).

Table 1
The capability of phospholipids to form the honeycomb-patterned structure on PLA film

	Phospholipids	5 wt%[a]	10 wt%	20 wt%
DLPC	(R_1, $R_2 = C_{11}H_{22}$, $R_3 = N^+(CH_3)_3$)	Phase separation	Phase separation	Phase separation
DMPC	(R_1, $R_2 = C_{13}H_{26}$, $R_3 = N^+(CH_3)_3$)	Phase separation	Phase separation	Phase separation
DPPC	(R_1, $R_2 = C_{15}H_{30}$, $R_3 = N^+(CH_3)_3$)	Phase separation	Phase separation	Phase separation
DSPC	(R_1, $R_2 = C_{17}H_{34}$, $R_3 = N^+(CH_3)_3$)	Phase separation	Phase separation	Phase separation
DOPC	(R_1, $R_2 = C_{17}H_{32}$, $R_3 = N^+(CH_3)_3$)	Opaque	Opaque	Opaque
DMPE	(R_1, $R_2 = C_{13}H_{26}$, $R_3 = NH_3$)	n.d.[b]	n.d.	n.d.
DPPE	(R_1, $R_2 = C_{15}H_{30}$, $R_3 = NH_3$)	n.d.	n.d.	n.d.
DSPE	(R_1, $R_2 = C_{17}H_{34}$, $R_3 = NH_3$)	n.d.	n.d.	n.d.
DOPE	(R_1, $R_2 = C_{17}H_{32}$, $R_3 = NH_3$)	Honeycomb	Honeycomb	Honeycomb

[a]Surfactant concentration by weight based on the weight of PLA.
[b]n.d. = not dissolved in chloroform.

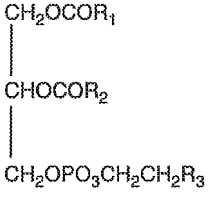

Phospholipid

2.2. Assessment of cell proliferation and adhesion

NIH3T3 cells (American Type Culture Collection, VA, USA) were used for assessing cell proliferation and adhesion on the honeycomb-patterned films. For the cell culture, sterilization of the honeycomb-patterned films was done by 70% ethanol washing. The cells were grown in Dulbecco's Modified Eagle Medium (DMEM; Invitrogen, Grand Island, CA, USA) supplemented with 10% heat-inactivated fetal bovine serum (FBS; Hyclone, UT, USA), penicillin (100 U/mL) and streptomycin (50 mg/mL). The cells were seeded on the honeycomb-patterned films coated on cover glasses (113 mm^2) at a density of 3.2×10^2 cells/cm^2 in a 12-well culture plate and cultured in a humidified environment of 5% CO_2 at 37 °C. After 24 and 48 h culture periods, the cell proliferations were measured by alamarBlue™ (Alamar Biosciences Inc., CA, USA) assay [16]. The alamarBlue™ was added to the wells in an amount equal to 10% of the total culture medium volume, and then the well was incubated for 2 h. Aliquots of 100 μL/sample were measured by a fluorescence plate reader (Wallac 1420 ARVOsx, PerkinElmer, Inc., MA, USA) set at excitation and emission wavelengths of 530 and 590 nm, respectively.

For assessing the cell adhesion on the honeycomb-patterned films, NIH3T3 cells were grown for 14 days and the media were changed every 2 days. Cell adhesions were observed by SEM (JSM-5310, JEOL, Tokyo, Japan) and FE-SEM, and the coverage of cells on the honeycomb-patterned film was calculated by image analysis software (nexusNewQube, Sumisho Electronics Co., Ltd., Tokyo, Japan).

2.3. Statistics

The data were expressed as means and standard deviations (SD). Comparisons of means between groups were performed by using the Student's unpaired *t*-test, and a p value of less than 0.05 was considered significant.

3. Results and discussion

Honeycomb-patterned films were prepared by a casting method from the polymer solution (5 mg/mL) under blowing with highly humid air at room temperature, and a phospholipid was used as the surfactant. Table 1 shows the capability of phospholipids to form the honeycomb-patterned structure on PLA film. PEs having saturated fatty acid moieties, such as DMPE, DPPE and DSPE, could not be dissolved in the polymer solution. DOPE (a PE having unsaturated fatty acid moieties), DOPC (a phosphatidylcholine having unsaturated fatty acid moieties) and all PC having saturated fatty acid moieties such as DLPC, DMPC, DPPC and DSPC were dissolved in the polymer solution. The solubility of each surfactant was checked visually. In this study, we used only soluble phospholipids for the honeycomb-patterned film fabrication. Film with PC having saturated fatty acid moieties, DLPC, DMPC, DPPC and DSPC, which were not observed to form the honeycomb-patterned structure on the surface, showed only phase separation. Film with phosphatidylcholine having unsaturated fatty acid moieties, DOPC, also did not form the honeycomb structure and only showed an opaque surface. DOPE was the only case in which PLA film showed the honeycomb-patterned structure on the surface. These phenomena were observed at surfactant concentrations of from 5% to 20% by weight based on the weight of PLA, as shown in Table 1.

The mechanism of the honeycomb-patterned formation has been described as follows: After placing a droplet of the polymer solution on the substrate, chloroform starts to evaporate. This leads to the cooling of the polymer solution and enables micron-size water droplets to condense onto the polymer solution. By evaporating the chloroform solution, the water droplets get close to being hexagonally packed. After evaporating the chloroform solution, the water droplets evaporate and the honeycomb-patterned structure is observed.

The balance between the alkyl chain length and size of the hydrophilic group of surfactants, as well as the solubility of the surfactants in the polymer solution, are important in fabricating the honeycomb-patterned film. DOPE has unsaturated alkyl chains and the volume of the hydrophilic group is comparatively smaller than that of PC. It has the advantage of forming reversed micelle structures in the water and oil phase [17]. DOPE as a surfactant contributes to the stability of the water droplets by self-assembly to the interface between the polymer solution and the water droplets. Moreover, DOPE is dissolved in PLA/chloroform solution easily owing to its structure of unsaturated alkyl chains. These two points, having unsaturated alkyl chains and a small hydrophilic area, and high solubility, are suitable for fabricating the honeycomb-patterned film. In this study, DOPE as a surfactant suits the PLA/chloroform solution for fabricating honeycomb-patterned film. Phospholipids are one of the major building blocks of the cell wall, and are safe and biodegradable. In addition, they are used for the drug delivery system, so this honeycomb-patterned film composed of poly(lactic acid) and DOPE is also safe and completely biodegradable.

We have examined the suitable concentration of DOPE for the honeycomb formation. Table 2 shows the relationship between the capability of the honeycomb-patterned structure and the DOPE concentration. When the

Table 2
The relationship between the capability to form the honeycomb-patterned structure and the concentration of DOPE

DOPE concentration[a] (wt%)	Honeycomb pattern	Pore diameter[b,c] (μm)
0.1	No uniform pattern	1–13
0.2	Honeycomb pattern	5.5±0.5
0.5	Honeycomb pattern	4.5±0.5
1	Honeycomb pattern	5.5±0.5
2	Honeycomb pattern	7±1
5	Honeycomb pattern	8±2
10	Honeycomb pattern	7±1
20	Honeycomb pattern	8±2
100	Not observed	—

[a]The concentration of DOPE by weight based on the weight of PLA.
[b]Pore diameters were estimated by optical microscope.
[c]Data were expressed as mean and standard deviations (SD), $n = 3$, except for the data of 0.1 wt% DOPE.

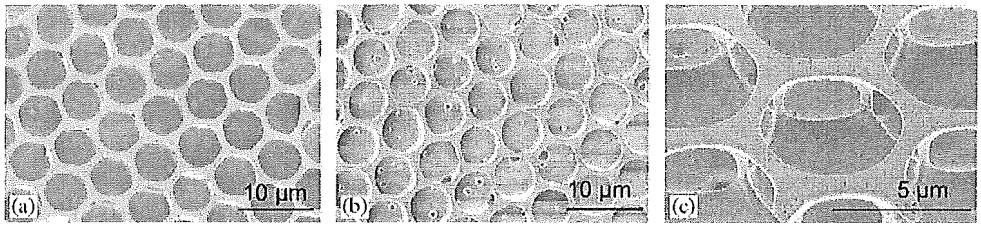

Fig. 1. FE-SEM images of the honeycomb-patterned films: (a) an image of the honeycomb-patterned film using DOPE as the surfactant (PLA–10%DOPE), bar = 10 μm, (b) an image of PLA–0.5%DOPE, bar = 10 μm and (c) a higher-magnification image of PLA–0.5%DOPE tilted at 40°, bar = 5 μm.

concentration of DOPE was from 0.2% to 20% by weight based on the weight of PLA, a uniform honeycomb-patterned structure was observed. The diameter of the honeycomb pore was from 6 to 10 μm when the concentration of DOPE was from 2 to 20 wt%. On the other hand, the diameter was from 4 to 6 μm when the concentration of DOPE was from 0.2 to 1 wt%. When the DOPE concentration was 0.1 wt%, no uniform pattern was observed, and the pore sizes varied from 1 to 13 μm (Table 2). On the contrary, when it was higher than 20 wt%, the honeycomb-pattern was not observed at all. It has been reported that more than 5 wt% of surfactant concentration was needed to fabricate the honeycomb-patterned structure of PLA when CAP was used [15]. By using DOPE, however, a lower amount and concentration can form the same structure on PLA film.

An FE-SEM image of the honeycomb structure of PLA–10%DOPE is shown in Fig. 1(a) and FE-SEM images of PLA–0.5%DOPE are shown in Fig. 1(b) and (c). Fig. 1(c) is the image of PLA–0.5%DOPE tilted at 40°. Uniform honeycomb structures are clearly observed as shown in Fig. 1(a) and (b). The pore size is around 5 μm, and the thickness of the honeycomb skeleton is about 1 μm. All pores are interconnected with each other (Fig. 1(c)).

The contact angles of water on the surface of the honeycomb-patterned PLA films are shown in Fig. 2. The water contact angles of non-washed PLA–DOPE were smaller than those of PLA–CAP, therefore, the surfaces of PLA–DOPE were supposed to be more hydrophilic than PLA–CAP. Additionally, the water contact angle decreased with an increase in the DOPE concentration. These findings suggest that DOPE may locate on the surface of the film. In order to prove this hypothesis, the surfaces of the honeycomb-patterned films were washed with ethanol, in which DOPE can be dissolved. This treatment dramatically increased the contact angle and decreased the hydrophilicity. The contact angles of PLA–DOPE after ethanol washing were as high as that of PLA–CAP at any concentration of DOPE.

NMR data supported the fact that ethanol washing reduced the content of DOPE. The content of DOPE was reduced to 30% in PLA–0.5%DOPE, and to 70% in PLA–2%DOPE. As each film contains 0.125 and 0.5 mg of DOPE, the residual DOPE is estimated to be 0.0375 and 0.35 mg, respectively. On the other hand, the content of

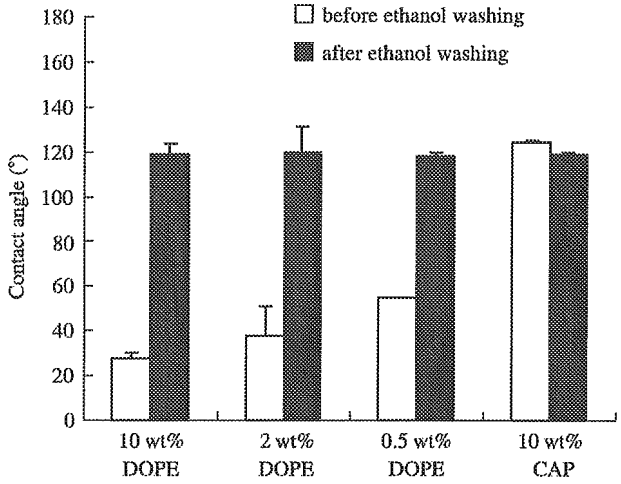

Fig. 2. Changes in water contact angles of various honeycomb-patterned films before ethanol washing (open columns) and after washing (closed columns). Data were expressed as mean and standard deviations (SD), $n = 3$.

CAP was hardly reduced in PLA–CAP after ethanol washing, and 95% of CAP (23.8 mg) remained.

A TOF-SIMS image also yielded evidence that DOPE exists on the surface of the honeycomb-patterned film. A TOF-SIMS image of DOPE fragments is shown in Fig. 3(a), PLA fragments are shown in Fig. 3(b), and the total ion fragments (merged image) are shown in Fig. 3(c). These results suggest that DOPE is condensed on the surface of the honeycomb-patterned film, and this phenomenon imparts a different hydrophilicity to each film depending on the content of DOPE. Therefore, the hydrophilicity of the honeycomb-patterned film can be controlled by the content of DOPE.

To examine the safety of the honeycomb-patterned PLA film, NIH3T3 cells were cultured on the film. Two films with different DOPE content (PLA–0.5%DOPE and PLA–2%DOPE) and PLA–10%CAP were examined. Ethanol washing was performed to sterilize the films before the cells were cultured. After 14 days of cell culture, NIH3T3 cells adhered to and covered the surface of the honeycomb-patterned film (PLA–2%DOPE), as shown in Fig. 4(a). On PLA–0.5%DOPE (Fig. 4(b)), some cells migrated through the pores of the honeycomb structure and adhered to the bottom surface of the

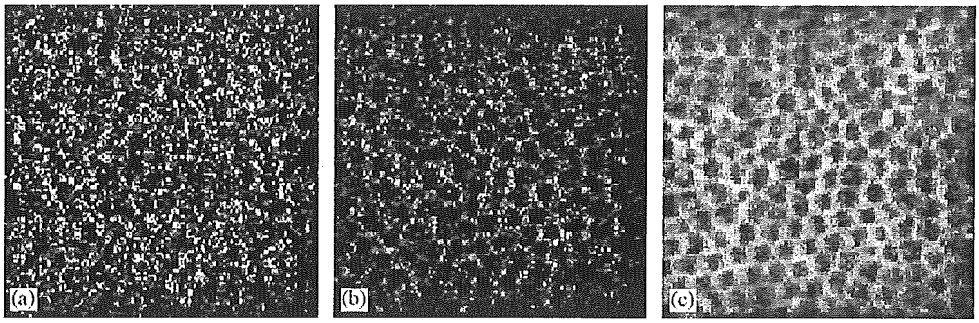

Fig. 3. TOF-SIMS images of the PLA–2%DOPE film: (a) DOPE ion image, (b) PLA ion image and (c) total ion image (merged image).

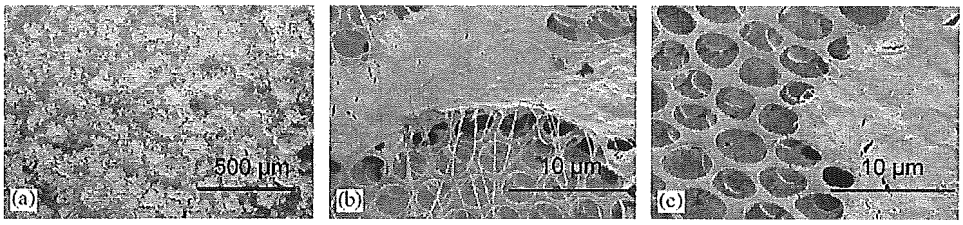

Fig. 4. (a) SEM image of NIH3T3 cells on the PLA–2%DOPE, bar = 500 μm, (b) FE-SEM image of the interaction between cells and the honeycomb-patterned structure (PLA–0.5%DOPE), and (c) FE-SEM image of the interaction between cells and the honeycomb-patterned structure (PLA–10%CAP) after 14 days of culture, bar = 10 μm.

honeycomb-patterned layer and fiber-like extracellular matrices, around 50 nm in diameter, expanded from the NIH3T3 cells. On the contrary, they did not spread from the cells on PLA–10%CAP (Fig. 4(c)). The area of the film covered with NIH3T3 cells was calculated using image analysis software. Sixty-six percent of the surface area of PLA–2%DOPE was covered with fibroblasts, 53% in PLA–0.5%DOPE and 28% in PLA–10%CAP. These data suggest that PLA–DOPE films are covered with cells via adhesion, and migration processes are comparatively faster than PLA–CAP film.

Moreover, cell proliferation was evaluated by alamarBlue™ assay and summarized in Fig. 5. After 24 h of cell culture, cell proliferation on PLA–0.5%DOPE was comparatively higher than that on PLA–2%DOPE and PLA–10%CAP ($p<0.05$). After 48 h, cell proliferation on PLA–0.5%DOPE was significantly higher than that on PLA–2%DOPE ($p<0.01$). It was clearly observed that cell proliferation on PLA–DOPE films was higher than PLA–CAP ($p<0.001$).

The cell proliferation assay revealed that PLA–DOPE films were better than PLA–CAP for NIH3T3 cell culture. DOPE is one of the major building blocks of the cell wall and is safe, as is clear from being used for the drug delivery system. On the other hand, CAP, a polymer derived from dodecylacrylamide and ω-carboxyhexylacrylamide, is broken down into acrylamide and other moieties. As the biocompatibility of acrylamide is still unclear, this difference might lead to better cell proliferation and adhesion on PLA–DOPE than on PLA–CAP.

It is well known that the pore size of artificial substrates has considerable influence on the cell behavior. For

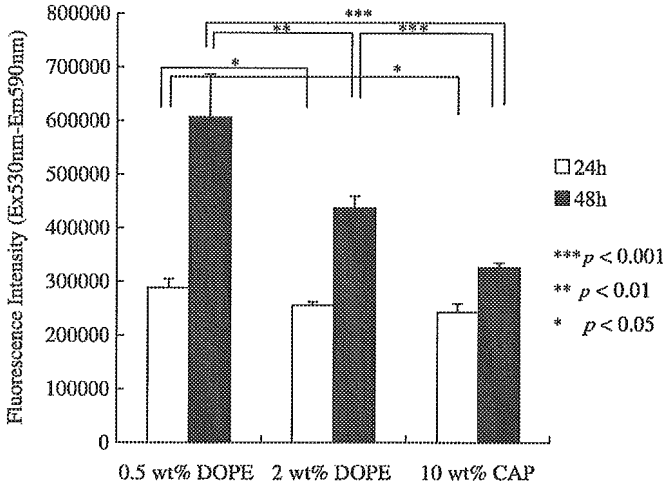

Fig. 5. Cell proliferation of NIH3T3 fibroblast cells cultured on honeycomb-patterned film assessed by alamarBlue™ assay. Data of 24 h (open columns) and 48 h (closed columns) cell cultures after they were expressed as mean and standard deviations (SD), $n = 3$ or 4.

example, the degree of spreading of hepatocyte was enhanced with the decrease of the pore size [18,19]. Moreover, the morphologies of neural cells could be changed by varying the pore size of the patterned films [20]. In this study, we used only 3-μm pore-size films for the cell culture, therefore further studies are required to confirm the relationship between cell behavior and the dimensions of the honeycomb structure in the case of DOPE as a surfactant.

Porous biodegradable polymer materials have been fabricated by various methods, such as phase separation,

salt leaching and freeze drying; however, the pore size is difficult to control by these methods. Our method is simple and can fabricate uniform pores. Moreover, our film is very thin and can be applied to any place. These characteristics can be advantages for application to tissue engineering. In other series of studies, we confirmed that the fine-structured pattern fabricated on the substrate had been kept for 3 weeks in a chondrocyte culture (data not shown).

4. Conclusions

In the present work, we found that DOPE is suitable as a new surfactant for fabricating micro-size honeycomb-patterned film among a series of phosphatidylcholines and phosphatidylethanolamines. The honeycomb-patterned PLA films were fabricated with concentrations of DOPE of from 0.2% to 20% by weight based on the weight of PLA. Contact-angle measurement and TOF-SIMS observation suggested that DOPE was concentrated and located on the surface of the honeycomb-patterned film. The content of DOPE can control the hydrophilicity of the film. Cell proliferation and adhesion on PLA–DOPE film were higher than on PLA–CAP. PLA–DOPE was demonstrated to be a good scaffold for cells such as NIH3T3.

Acknowledgements

We gratefully acknowledge our thanks to Masaya Ito for his kind help and advice, plus Hisao Moriya, Masahito Sato and Makiko Ikeda of the Institute for Structure Analysis, TEIJIN Limited, for the SEM, FE-SEM and TOF-SIMS observations, image analysis and helpful discussions.

References

[1] Yabu H, Tanaka M, Ijiro K, Shimomura M. Preparation of honeycomb-patterned polyimide films by self-organization. Langmuir 2003;19:6297–300.
[2] Cho CH, Ihm SK. Development of new vanadium-based oxide catalysts for decomposition of chlorinated aromatic pollutants. Environ Sci Technol 2002;36:1600–6.
[3] Tanaka M, Takebayashi M, Miyama M, Shimomura M. Fabrication of regular porous polymer films for biomedical devices—control of pore structure and size. In: Third Asian international symposium on biomaterials and drug delivery systems, Taipei, 2002. p. 105–8.
[4] Tanaka M, Takebayashi M, Miyama M, Nishida J, Shimomura M. Design of novel biointerfaces (II). Fabrication of self-organized porous polymer film with highly uniform pores. Biomed Mater Eng 2004;14:439–46.
[5] Nishikawa T, Nishida J, Ookura R, Nishimura S, Wada S, Karino T, et al. Honeycomb-patterned thin films of amphiphilic polymers as cell culture substrates. Mater Sci Eng C 1999;8-9:495–500.
[6] Ookura R, Nishida J, Nishikawa T, Shimomura M. Stabilization of micropatterned polymer films as artificial extracellular matrices for tissue engineering. Mol Cryst Liq Cryst 1999;337:461–4.
[7] Nishikawa T, Nishida J, Nishikawa K, Ookura R, Ookubo H, Kamachi H, et al. Novel cell culture substrates based on microporous films of amphiphilic polymers. In: Iwasawa Y, Oyama N, Kunieda H, editors. The international conference on colloid and surface science; 2000. Tokyo: Elsevier Science Ltd.; 2000. p. 509–12.
[8] Manz A, Becker H. Microsystem technology in chemistry and life sciences, Springer Desktop editions in chemistry. Berlin: Springer; 1999.
[9] Xia Y, Whitesides GM. Soft lithography. Angew Chem, Int Ed 1998; 37:550–75.
[10] Lo H, Kadiyala S, Guggino SE, Leong KW. Poly(L-lactic acid) foams with cell seeding and controlled-release capacity. J Biomed Mater Res 1996;30:475–84.
[11] Widawski G, Rawiso M, François B. Self-organized honeycomb morphology of star-polymer polystyrene films. Nature 1994;369: 386–9.
[12] Maruyama N, Koito T, Nishida J, Sawadaishi T, Cieren X, Ijiro K, et al. Mesoscopic patterns of molecular aggregates on solid substrates. Thin Solid Films 1998;327–329:854–6.
[13] Shimomura M, Sawadaishi T. Bottom-up strategy of materials fabrication: a new trend in nanotechnology of soft materials. Curr Opin Colloid Interf Sci 2001;6:11–6.
[14] Confirmed by 1H-NMR, A-600, JEOL, Tokyo, Japan.
[15] Nishikawa T. Preparation and application prospects of porous polymer thin films. In: Polymer frontier 21 speciality polymer. Japan: The Society of Polymer Science; 2003. p. 111–48.
[16] Lancaster MV, Fields RD. Antibiotic and cytotoxic drug susceptibility assays using resazurin and poising agents patent US5501959. 1996.
[17] Israelachvili JN. Intermolecular and surface forces. London: Academic Press; 1992.
[18] Sato K, Hasebe K, Tanaka M, Takebayashi M, Nishikawa K, Shimomura M, et al. Preparation of the honeycomb-patterned porous film of biodegradable polymer for tissue engineering scaffolds. Int J Nanosci 2002;1:689–93.
[19] Tanaka M, Nishikawa K, Kawai T, Matsushita M, Todo S, Shimomura M, et al. Control of hepatocyte adhesion and function on self-organized honeycomb-patterned polymer film. Colloids and Surf. A, in press.
[20] Tsuruma A, Tanaka M, Fukushima N, Shimomura M. Morphological changes in neurons by self-organized patterned films. e-J Surf Sci Nanotechnol 2005;3:159–64.

TISSUE ENGINEERING
Volume 11, Number 7/8, 2005

Augmented Bone Regeneration Activity of Platelet-Rich Plasma by Biodegradable Gelatin Hydrogel

AKISHIGE HOKUGO, D.D.S., Ph.D.,[1] MAKOTO OZEKI, M.Eng.,[1]
OSAMU KAWAKAMI, M.D.,[1] KEISUKE SUGIMOTO, D.D.S., Ph.D.,[2]
KOZO MUSHIMOTO, D.D.S., Ph.D.,[2] SHOSUKE MORITA, D.D.S., Ph.D.,[2]
and YASUHIKO TABATA, Ph.D., D.Med.Sci., D.Pharm.[1]

ABSTRACT

This study investigates the ability of platelet-rich plasma (PRP) combined with biomaterials to enhance *in vivo* bone-repairing activity. A biodegradable hydrogel was prepared from gelatin, which has an affinity for various growth factors. Rabbit PRP was conventionally prepared by blood centrifugation and dropped onto freeze-dried gelatin hydrogel to obtain gelatin hydrogel incorporating PRP. Gelatin hydrogel incorporating PRP was applied to a bone defect of rabbit ulna to evaluate bone formation at the defect in terms of soft X-ray and histological examinations. As controls, fibrin incorporating PRP, empty gelatin hydrogel, and free PRP were applied to the defect; in addition, defect without any application was examined. Successful bone regeneration was observed at bone defect treated with gelatin hydrogel incorporating PRP, in marked contrast to the control groups. When in contact with gelatin, growth factors, such as platelet-derived growth factor and transforming growth factor β_1, were released from the PRP. PRP growth factors are immobilized in the hydrogel through physicochemical interaction with gelatin molecules. The immobilized growth factors are released from the hydrogel in concert with hydrogel degradation. It is likely that the gelatin hydrogel permitted the controlled release of bioactive growth factors, resulting in factor-induced promotion of bone regeneration.

INTRODUCTION

BASIC STUDIES have been conducted on growth factors, which function in the repair and regeneration of tissues.[1,2] Platelet-derived growth factor (PDGF) and basic fibroblast growth factor (bFGF) are clinically available for therapeutic applications to skin wounds.[3,4] It is well recognized that the specialized secretory granules of platelets, the α granules, contain growth factors, such as PDGF, transforming growth factor β (TGF-β), insulin-like growth factor I (IGF-I), epidermal growth factor (EGF), and endothelial cell growth factor (ECGF).[5] These growth factors are released from platelets when they are activated by a stimulus or aggregated by some activators.[6,7] Among them, TGF-β and PDGF promote the healing of soft and bone tissues through stimulation of collagen production to improve wound strength and initiation of callus formation.[8–10] Thus, if platelet growth factors can effectively function at wound tissue, growth factor-induced acceleration of wound healing may be expected. Such an application of platelets present in platelet-rich plasma (PRP) has begun in the field of dentistry.[11,12] It is expected that the biological effect of multiple growth factors on the enhancement of tissue regeneration and repair is higher than that of a single growth factor. Some research has been performed to demonstrate

[1]Department of Biomaterials, Field of Tissue Engineering, Institute for Frontier Medical Sciences, Kyoto University, Kyoto, Japan.
[2]First Department of Oral and Maxillofacial Surgery, Osaka Dental University, Osaka, Japan.

the activity of PRP combined with biomaterials to promote bone regeneration.[13–15] However, it is questionable whether combination with biomaterials allows PRP to enhance biological activity.[16–18] Little statistical analysis has been performed to confirm the therapeutic efficacy. In addition, there is no clear scientific explanation for the role played by the biomaterials in PRP-induced augmentation of bone repairing.[19] It is apparent from research that a combination of appropriate biomaterials is required to enhance the biological function of PRP. However, little has been done to investigate the biological function of PRP from the viewpoint of combination materials.

Gelatin is a biodegradable material that has been extensively utilized for pharmaceutical and medical purposes and proven to be biosafe throughout its long history of clinical applications.[20] It is known that the isoelectric point (IEP) of gelatin is changed by the conditions of its preparation from collagen. A biodegradable hydrogel, prepared from "acidic" gelatin with an IEP of 5.0, can ionically interact with "basic" growth factors with IEPs higher than 8.5. For this hydrogel system, any growth factor immobilized in the hydrogel of acidic gelatin is released only when the hydrogel is degraded to generate water-soluble gelatin fragments. Using the gelatin hydrogel, we have achieved the controlled release of bFGF,[21] TGF-β_1,[22] PDGF,[23] and bone morphogenetic protein 2 (BMP-2)[24] to enhance their biological functions.[25,26]

The objective of the present study is to investigate the potentiality of gelatin hydrogel as a release carrier of PRP growth factors. We examine the effect of gelatin hydrogel incorporating PRP on the promotion of bone regeneration with a rabbit model of ulna defect.

MATERIALS AND METHODS

Materials

A gelatin sample with an IEP of 5.0 was kindly supplied by Nitta Gelatin (Osaka, Japan) and Tisseel of fibrin glue was kindly supplied from Baxter (Vienna, Austria). Glutaraldehyde (GA), glycine, and other chemicals were purchased from Wako Pure Chemical Industries (Osaka, Japan) and used without further purification.

Preparation of gelatin hydrogels

Gelatin hydrogels were prepared by chemical cross-linking of gelatin aqueous solution as reported previously.[21] Briefly, after mixing 70 μL of aqueous GA solution (25 wt%) with 40 mL of aqueous gelatin solution (5 wt%) preheated at 40°C, the mixed aqueous solution was cast into a 96-well multiwell culture plate (Corning Life Sciences, Acton, MA) and left for 12 h at 4°C to allow the chemical cross-linking of gelatin. The resulting hydrogel rods (6 mm in diameter and 10 mm thick) were placed in 50 mL of 100 mM glycine aqueous solution, followed by agitation at 37°C for 1 h to block the residual aldehyde groups of unreacted GA. The cross-linking hydrogel rods were then washed twice with doubly distilled water, freeze-dried, and sterilized with ethylene oxide gas. The water content of gelatin hydrogel (the weight ratio of water present in the hydrogel relative to the wet hydrogel) was 98 wt%, when calculated from the hydrogel weight before and after swelling in 0.5 mM phosphate-buffered saline solution (PBS, pH 7.4) for 24 h at 37°C.

Preparation of platelet-rich plasma

Fifteen Japanese White rabbits ranging from 3.0 to 3.5 kg in body weight (Shimizu Laboratory Animal Supplies, Kyoto, Japan) were used. All the animal experiments were approved by the Kyoto University Committee for Animal Experimentation. Briefly, rabbits were anesthetized by intramuscular injection of 10 mL of ketamine hydrochloride (Ketalar; Sankyo Seiyaku, Tokyo, Japan) mixed with 5 mL of xylazine (Celactal; Bayer, Tokyo, Japan) at a dose of 0.65 mL/kg body weight. PRP was prepared according to a method previously reported.[27] Briefly, 10 mL of blood was freshly obtained from 25 rabbits, using a syringe containing 1 mL of acid citrate dextrose-A (ACD-A) solution as an anticoagulant. The blood was centrifuged in a laboratory centrifugation apparatus (RSL-05A; Sakuma, Tokyo, Japan) at 4°C for 10 min at 2400 rpm. Subsequently, the yellow plasma containing the platelet fraction was collected and further centrifuged at 4°C for 10 min at 3600 rpm to separate the platelets. Platelet-poor plasma (PPP) was prepared by exclusion of the PRP fraction from the buffy coat. The approximate volume of PRP obtained was 0.8 mL. Platelet counts were performed for samples of peripheral blood, PPP, and PRP with an automated hematology analyzer (SE9000; Sysmex, Kobe, Japan).

To examine the types of growth factor secreted from PRP, culture dishes (Corning Life Sciences) were coated with 0.1% gelatin solution and thrombin (6 mg/mL). The coating was performed by placing the protein solution in the culture dishes, leaving them at 37°C for 1 h, and subsequently rinsing them with PBS. PRP (200 μL) was then added to the dishes prepared. (As controls, PRP [200 μL] was added to uncoated glass or polystyrene culture dishes). After leaving them for 1 h at 37°C to allow platelet activation, 200 μL of PBS was added and then 100 μL of the supernatant was obtained to measure the concentration of PDGF-BB and TGF-β_1 by enzyme-linked immunosorbent assay (ELISA), using a PDGF-BB ELISA kit (R&D Systems, Minneapolis, MN) and a TGF-β_1 ELISA kit (R&D Systems).

Preparation of gelatin hydrogel and fibrin glue incorporating PRP

PRP (200 μL) was dropped onto freeze-dried gelatin hydrogel rods and left for 1 h at 37°C to allow the PRP to impregnate the hydrogel. As a control, PRP-free, empty gelatin hydrogels were prepared similarly other than using PBS. Fibrin glue was prepared conventionally by mixing fibrinogen and thrombin solution, and 200 μL of PRP was added to the fibrin glue.

In vivo experiment

The *in vivo* experiment was performed by a surgical procedure previously reported,[28] with modification. The site to be operated, either the left or right front limb of rabbits, was shaved, prepped, and draped for aseptic surgery in the supine position. A 2-cm-long superomedial incision was made and the tissue overlying the diaphysis of the radius was dissected. A 1-cm segmental defect was prepared in the radius with a surgical oscillating saw supplemented by copious sterile saline water irrigation (Fig. 1A). Gelatin hydrogel incorporating 200 μL of PRP, fibrin glue incorporating 200 μL of PRP, empty gelatin hydrogel, and 200 μL of free PRP were applied to defects, and some defects were left without any application. Fixation of the ostectomized bone was unnecessary because of the fibro-osseous union between the ulna and radius located distal and proximal to the surgical site (Fig. 1B).

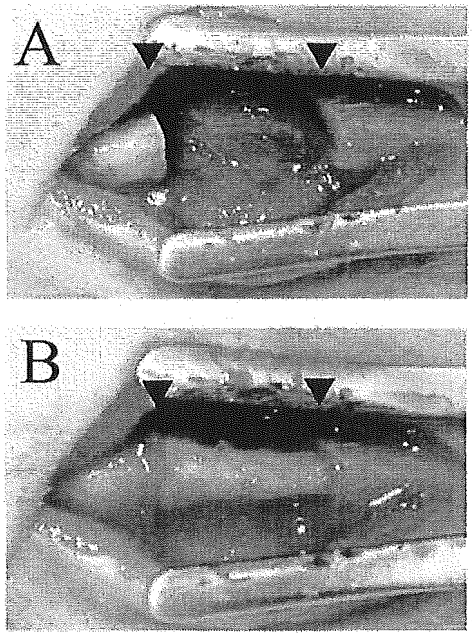

FIG. 1. (**A**) A 1-cm segmental defect was made in the ulna of rabbits. (**B**) Gelatin hydrogel incorporating PRP was applied to the defect. Arrowheads indicate the edge of ulna bone resected.

The soft tissue was approximated with interrupted 4-0 Vicryl (Ethicon, Somerville, NJ) and the skin was closed with 3-0 silk sutures. A postoperative antibiotic (fostomycin) ([Fosmicin]; Meiji Seika, Tokyo, Japan) was administered intramuscularly at a dose of 100 mg/kg per day for 3 days. The radius–ulna complex containing the defect was then taken out and fixed in 10 w% formaldehyde solution in PBS for assessment of bone regeneration.

Assessment of bone regeneration

Bone regeneration at the site of bone defect was assessed by soft X-ray, dual-energy X-ray absorptometry (DEXA), and histological examinations 4 weeks after application. Soft X-ray photographs of bone specimens were taken with a soft X-ray system (CBM-2; Softex, Tokyo, Japan) at 25 kV and 2.5 mA for 20 s. The bone mineral density (BMD) of each bone defect was measured at the 5×5 mm^2 region of interest by DEXA with a bone mineral analyzer (DSC 600EX-III; Aloka, Tokyo, Japan). This instrument was calibrated with a phantom of known mineral content. Each scan was performed at a speed of 20 mm/s and the scanning length was 1 mm.

Bone specimens were placed into 10% neutral phosphate-buffered formaldehyde, decalcified with 10% formic acid, and processed for paraffin embedding. Sections (3 μm thick) were prepared and stained with hematoxylin and eosin to view by light microscopy (AX80T; Olympus, Tokyo, Japan).

Statistical analysis

All data were statistically analyzed, using the Fisher least significant difference test for multiple comparisons, and statistical significance was accepted as less than 0.05. Experimental results were expressed as means ± the standard deviation of the mean.

RESULTS

Platelet activation

Figure 2 shows the number of platelets generated during the process of PRP preparation. The platelet number in PRP was significantly high compared with that of blood, indicating that the preparation process worked well to concentrate platelets from the blood sample.

Figure 3 shows PDGF-BB and TGF-β_1 content in the soluble fraction of PRP after exposure to various dishes. It is apparent that similar amounts of PDGF-BB and TGF-β_1 were released from PRP after exposure to gelatin-coated, thrombin-coated, and glass dishes. On the other hand, the amount of PDGF-BB and TGF-β_1 released from PRP exposed to noncoated culture dishes was significantly lower than that of other dishes.